Alkylation

International Edition: DOI: 10.1002/anie.201914061
German Edition: DOI: 10.1002/ange.201914061

Regioselective Hydroalkylation and Arylalkylation of Alkynes by Photoredox/Nickel Dual Catalysis: Application and Mechanism

*Huifeng Yue[+], Chen Zhu[+], Rajesh Kancherla, Fangying Liu, and Magnus Rueping**

Abstract: *Alkynes are an important class of organic molecules due to their utility as versatile building blocks in synthesis. Although efforts have been devoted to the difunctionalization of alkynes, general and practical strategies for the direct hydroalkylation and alkylarylation of terminal alkynes under mild reaction conditions are less explored. Herein, we report a photoredox/nickel dual-catalyzed anti-Markovnikov-type hydroalkylation of terminal alkynes as well as a one-pot arylalkylation of alkynes with alkyl carboxylic acids and aryl bromides via a three-component cross-coupling. The results indicate that the transformations proceed via a new mechanism involving a single-electron transfer with subsequent energy-transfer activation pathways. Moreover, steady-state and time-resolved fluorescence-spectroscopy measurements, density functional theory (DFT) calculations, and wavefunction analysis have been performed to give an insight into the catalytic cycle.*

Introduction

The development of improved methods for the efficient construction of multiple carbon–carbon and/or carbon–heteroatom bonds in one synthetic operation is of great interest. In this context, the potential of multi-component reactions (MCRs) as a tool to increase efficiency, productivity, reduce costs, and decrease the environmental impact has been long recognized.[1] Furthermore, multi-component reactions are highly attractive as they allow the assembly of complex structures starting from simple starting materials. The feasibility of MCRs in the functionalization of carbon–carbon triple bonds, which are ubiquitous in organic compounds, has been confirmed especially in the synthesis of heterocycles.[2] In contrast, the application of MCRs to the dicarbofunctionalization of readily accessible terminal alkynes, affording structurally defined multi-substituted alkenes, has been rarely realized.[3] Moreover, alternative protocols require the use of organo-metal species and multistep transformations.[4] Therefore, it is desirable to develop general, efficient, and practical protocols for the dicarbofunctionalization of terminal alkynes.[5]

In addition to dicarbofunctionalization, the hydrocarbofunctionalization of terminal alkynes is a fundamental transformation leading to valuable substituted alkene products. While the hydroarylation of terminal alkynes has been established,[6] hydroalkylation is rare.[7] Thus, the development of general, efficient, and practical protocols for the hydroalkylation of terminal alkynes would be an important advancement.

Recently, photo-mediated transition-metal catalysis has emerged as a powerful method in organic synthesis.[8] In particular, photoredox/nickel dual catalysis shows advantages and important products have been afforded by using this strategy.[9] Notably, photoredox/nickel dual catalysis has recently found application in the hydroalkylation of terminal and internal alkynes.[10,11] Considerable progress has been made by the Wu group to realize the hydroalkylation of internal alkynes with ether and amide C(sp^3)–H bonds with high selectivity.[10] During the course of this work, a decarboxylative hydroalkylation of aliphatic alkynes with alkyl carboxylic acids was achieved, giving the corresponding product in Markovnikov regioselectivity.[11] However, protocols for the hydroalkylation of alkynes, especially with the opposite regioselectivity, are still lacking.

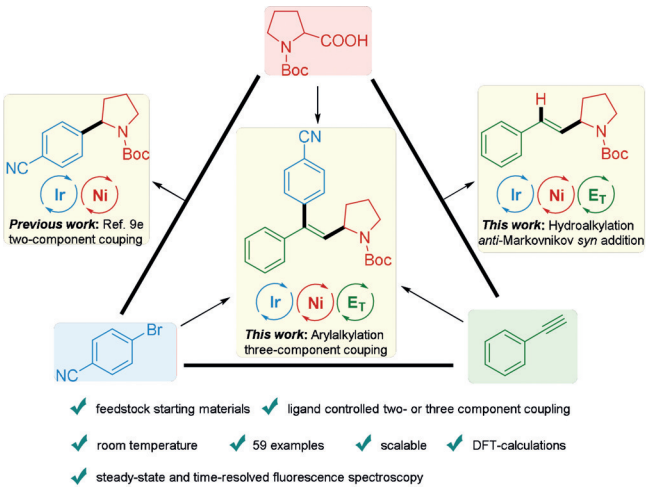

Scheme 1. Photoredox/nickel dual-catalyzed transformations involving aryl bromides, carboxylic acids, and alkynes.

[*] H. Yue,[+] C. Zhu,[+] R. Kancherla, Prof. Dr. M. Rueping
King Abdullah University of Science and Technology (KAUST)
KAUST Catalysis Center (KCC)
Thuwal, 23955-6900 (Saudi Arabia)
E-mail: Magnus.Rueping@kaust.edu.sa
H. Yue,[+] C. Zhu,[+] F. Liu, Prof. Dr. M. Rueping
Institute of Organic Chemistry, RWTH Aachen University
Landoltweg 1, 52074 Aachen (Germany)
[+] These authors contributed equally to this work.
Supporting information and the ORCID identification number(s) for the author(s) of this article can be found under: https://doi.org/10.1002/anie.201914061.

Despite the significant progress made in photoredox and transition-metal dual-catalyzed two-component cross-coupling reactions, less is known about challenging multi-component cross-couplings via this dual catalysis. Considering the great significance of the one-pot difunctionalization of alkynes, we herein report a photoredox/nickel dual-catalyzed anti-Markovnikov-type hydroalkylation of alkynes as well as the one-pot arylalkylation of alkynes with alkyl carboxylic acids and aryl bromides via three-component cross-coupling under mild conditions (Scheme 1). A wide range of disubstituted and trisubstituted olefin products have been accessed in a *syn*-addition manner, which is difficult to achieve using traditional methods. This protocol features the utilization of feedstock starting materials, mild reaction conditions, high functional-group tolerance, complex molecular applications, successful scale-up, and a novel mechanism involving single-electron transfer (SET) and energy-transfer (E_T) activation pathways.

Results and Discussion

We initiated our study by finding suitable conditions for the catalytic hydroalkylation of alkynes using ethynylbenzene **1a** and Boc-Pro-OH **2a** as model substrates, Cs_2CO_3 as base, Pc1 as photocatalyst, $NiCl_2$·glyme as the nickel source, and DMF as solvent, which afforded the corresponding anti-Markovnikov-type hydroalkylation product **3a** in 31 % yield only (Table 1, entry 1). Various solvents were evaluated next, and acetonitrile was found to give a slightly higher yield and stereoselectivity (entries 2–4). When other bases were used, the reaction did not occur or took place with lower yields (entries 5–7). The photocatalyst screening revealed that Pc4 gives the product with higher stereoselectivity without decreasing the yield (entries 8–12). Several commonly used nickel catalysts were evaluated next; however, no further improvement was observed (entries 13–16). Using 10 equiv of H_2O as an additive decreased the yield (entry 17). Finally, the best yield (72 %) was obtained after adjusting the amount of radical precursor and base, and performing the reaction in a mixture of solvents for a prolonged reaction time (entries 18 to 20). Using 10 mol % dtbbpy as ligand decreased the yield and the stereoselectivity (entry 21). Reducing the amount of carboxylic acid **2a** to 1 equiv slightly decreased the yield (57 % yield, entry 22), while adding 2 equiv of H_2O was beneficial for the formation of the desired product (65 % yield, entry 23). Control experiments were conducted, and no product was obtained in the absence of the nickel catalyst and photocatalyst (entries 24 and 25).

With the optimized reaction conditions in hand, the scope of the alkyne hydroalkylation with respect to both reaction partners was evaluated (Table 2). A series of electronically and sterically diverse terminal alkynes could be converted into the corresponding disubstituted alkenes in moderate to high yields. Although ethynylbenzenes bearing a methyl group in the *para*- and *meta*-position underwent this transformation in good yields, *ortho*-methyl-substituted ethynylbenzene gave the corresponding product in moderate yield only, indicating that the process can be hampered by steric hindrance (**3b**–**3d**). Alkynes possessing electron-donating and electron-withdrawing functional groups such as methoxy,

Table 1: Reaction conditions for the optimization of the photoredox/nickel dual-catalyzed hydroalkylation of alkynes.

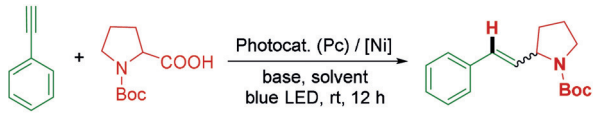

1a **2a** **3a**

Entry[a]	Pc	[Ni]	Base	Solvent	Yield (%)[b]
1	Pc1	$NiCl_2$·glyme	Cs_2CO_3	DMF	31 (60:40)
2	Pc1	$NiCl_2$·glyme	Cs_2CO_3	CH_3CN	32 (66:34)
3	Pc1	$NiCl_2$·glyme	Cs_2CO_3	DMSO	28 (60:40)
4	Pc1	$NiCl_2$·glyme	Cs_2CO_3	acetone	31 (63:37)
5	Pc1	$NiCl_2$·glyme	K_2CO_3	CH_3CN	31 (63:37)
6	Pc1	$NiCl_2$·glyme	Na_2CO_3	CH_3CN	16 (60:40)
7	Pc1	$NiCl_2$·glyme	Li_2CO_3	CH_3CN	0
8	Pc2	$NiCl_2$·glyme	Cs_2CO_3	CH_3CN	9 (71:29)
9	Pc3	$NiCl_2$·glyme	Cs_2CO_3	CH_3CN	15 (69:31)
10	Pc4	$NiCl_2$·glyme	Cs_2CO_3	CH_3CN	32 (73:27)
11	Pc5	$NiCl_2$·glyme	Cs_2CO_3	CH_3CN	10 (63:37)
12	Pc6	$NiCl_2$·glyme	Cs_2CO_3	CH_3CN	9 (60:40)
13	Pc4	$Ni(cod)_2$	Cs_2CO_3	CH_3CN	24 (73:27)
14	Pc4	$NiBr_2$	Cs_2CO_3	CH_3CN	23 (72:28)
15	Pc4	$Ni(acac)_2$	Cs_2CO_3	CH_3CN	12 (75:15)
16	Pc4	$Ni(OAc)_2·4H_2O$	Cs_2CO_3	CH_3CN	18 (74:26)
17[c]	Pc4	$NiCl_2$·glyme	Cs_2CO_3	CH_3CN	20 (73:27)
18[d]	Pc4	$NiCl_2$·glyme	Cs_2CO_3	CH_3CN	45 (73:27)
19[e]	Pc4	$NiCl_2$·glyme	Cs_2CO_3	CH_3CN + DMF	54 (73:27)
20[f]	**Pc4**	**$NiCl_2$·glyme**	**Cs_2CO_3**	**CH_3CN + DMF**	**72 (73:27)**
21[f,g]	Pc4	$NiCl_2$·glyme	Cs_2CO_3	CH_3CN + DMF	15 (68:32)
22[h]	Pc4	$NiCl_2$·glyme	Cs_2CO_3	CH_3CN + DMF	57 (73:27)
23[h,i]	Pc4	$NiCl_2$·glyme	Cs_2CO_3	CH_3CN + DMF	65 (73:27)
24[e]	Pc4	–	Cs_2CO_3	CH_3CN + DMF	0
25[e]	–	$NiCl_2$·glyme	Cs_2CO_3	CH_3CN + DMF	0

[a] Reaction conditions: ethynylbenzene (0.1 mmol), Boc-Pro-OH (0.2 mmol), photocatalyst (0.001 mmol), [Ni] (0.01 mmol), base (0.2 mmol) in solvent (2.0 mL) at room temperature under irradiation with a 34 W blue LED for 12 h. [b] GC yield and calibrated *Z*/*E*-ratio using (*E*)-stilbene as internal standard. [c] H_2O (10 equiv) was added. [d] Boc-Pro-OH (5 equiv) and Cs_2CO_3 (5 equiv) in 5 mL CH_3CN, 24 h. [e] Boc-Pro-OH (5 equiv) and Cs_2CO_3 (5 equiv) in 2.5 mL CH_3CN and 2.5 mL DMF, 24 h. [f] Boc-Pro-OH (3 equiv) and Cs_2CO_3 (1 equiv) in 2.5 mL CH_3CN and 2.5 mL DMF, 48 h. [g] With 10 mol % dtbbpy as ligand. [h] Boc-Pro-OH (1 equiv) and Cs_2CO_3 (1 equiv) in 2.5 mL CH_3CN and 2.5 mL DMF, 48 h. [i] H_2O (2 equiv) was added. Pc = photocatalyst.

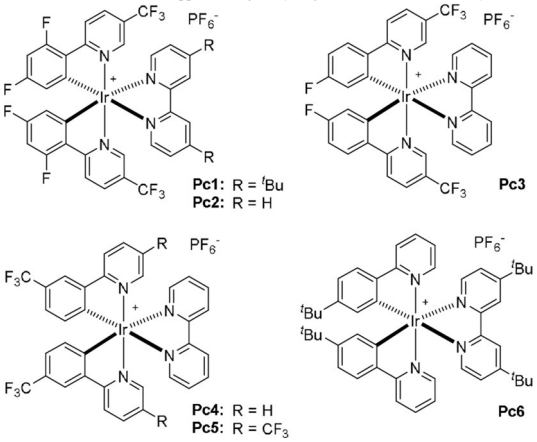

Table 2: Substrate scope for the photoredox/nickel dual-catalyzed hydroalkylation of alkynes.[a]

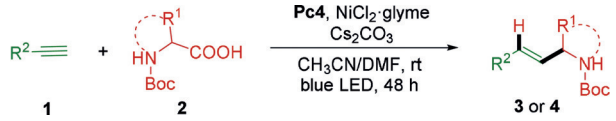

Alkyne scope

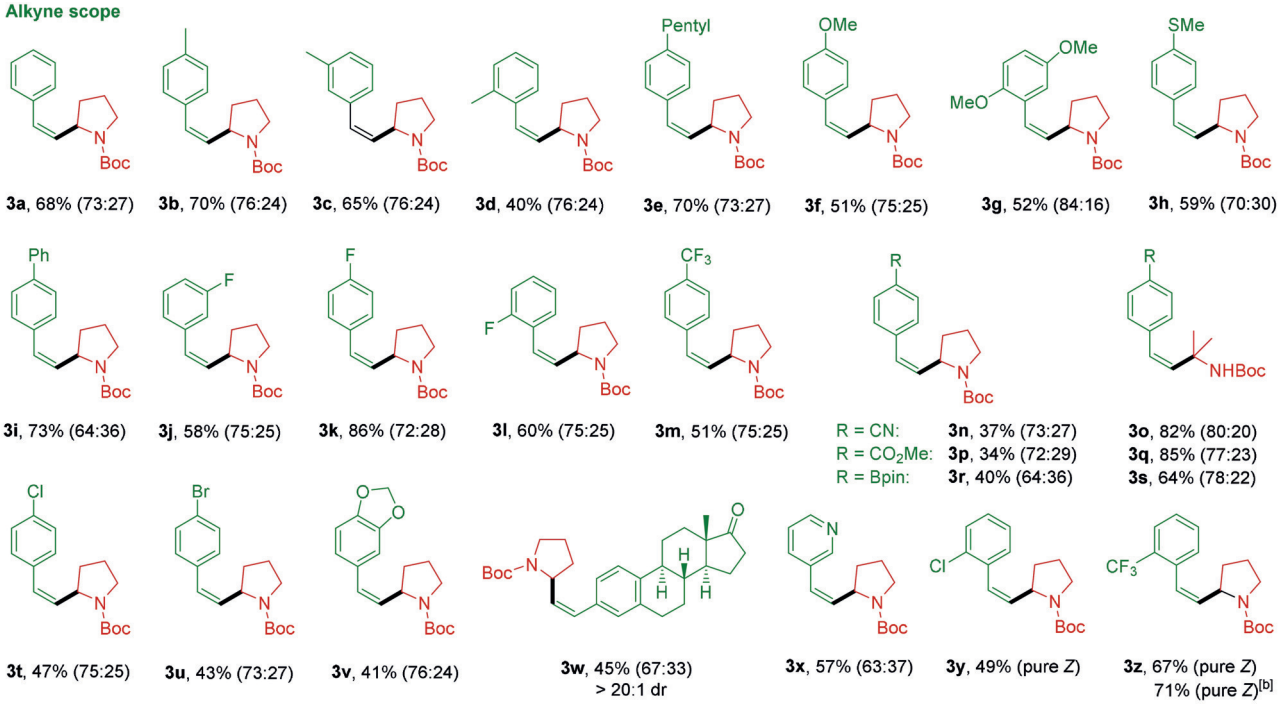

Carboxylic acid scope

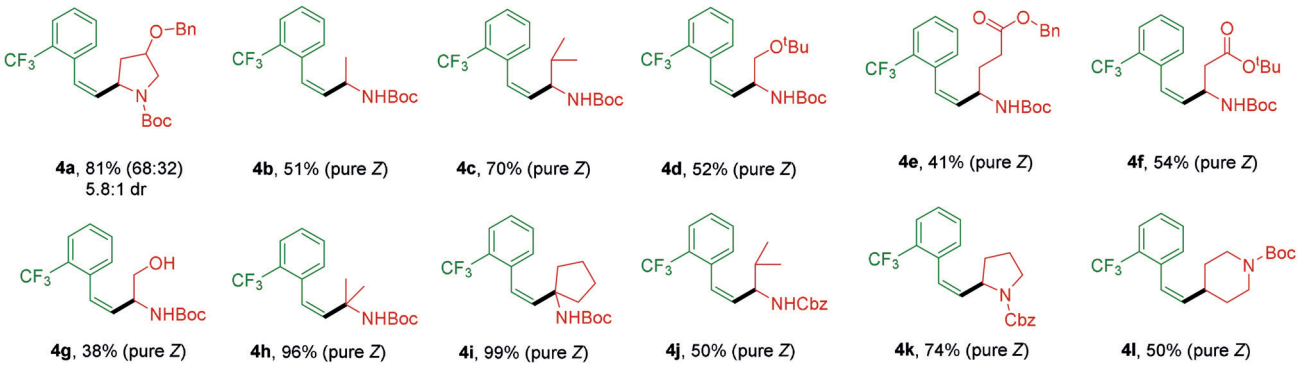

[a] Reaction conditions: alkyne (0.1 mmol), alkyl carboxylic acid (0.3 mmol), Pc4 (0.001 mmol), $NiCl_2$·dme (0.01 mmol), Cs_2CO_3 (0.1 mmol) in DMF (2.5 mL) and CH_3CN (2.5 mL) at room temperature under irradiation with a 34 W blue LED for 48 h. The values in parenthesis represent the *Z*/*E*-ratio of the product determined by ^1H NMR analysis. [b] The reaction was performed on a 2.0 mmol scale.

methylthio, fluoro, trifluoromethyl, cyano, and ester groups were all suitable substrates for this transformation (**3f–3h** and **3j–3q**). Importantly, some potentially sensitive groups such as borate ester, chloride, and even bromide were well tolerated under our reaction conditions, allowing further functionalization of the generated products **3r–3u**. Although substrates bearing electron-withdrawing functional groups reacted with Boc-Pro-OH in only moderate yields (**3n**, **3p**, and **3r**), good to high yields and better stereoselectivity were obtained when they reacted with a tertiary amino acid (**3o**, **3q**, and **3s**). Also, product **3v** bearing a bicyclic residue was obtained in moderate yield. Moreover, this protocol could be readily extended to estrone- and heterocycle-derived alkynes. Notably, chloride and trifluoromethyl functional groups in *ortho*-position on the phenyl residue of ethynylbenzene improved the stereoselectivity of the transformation significantly, giving pure *Z*-isomers of the corresponding products (**3y** and **3z**). Notably, **3z** was obtained as *Z*-isomer in a good yield of 71% when the reaction was conducted on a 2.0 mmol scale, showing the scalability and practicability of this newly developed mild hydroalkylation protocol.

Next, the scope of alkyl carboxylic acids was explored. A wide range of Boc-protected cyclic and acyclic secondary amino acids bearing alkyl, ether, ester, and even unprotected

Table 3: Substrate scope for the photoredox/nickel dual-catalyzed arylalkylation of alkynes.[a]

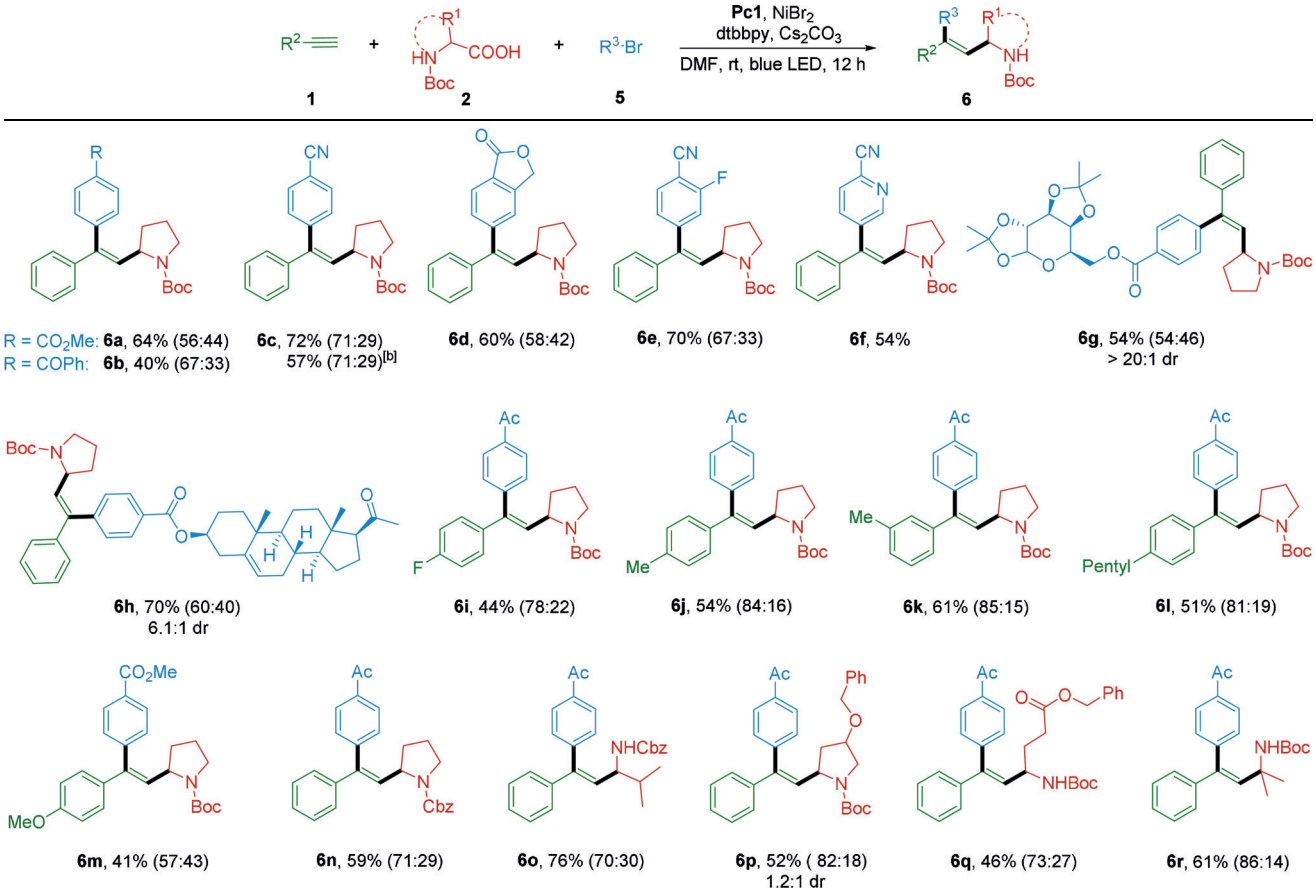

[a] Reaction conditions: aryl bromide (0.2 mmol), alkyl carboxylic acid (0.4 mmol), alkyne (0.6 mmol), Pc1 (0.002 mmol), $NiBr_2$ (0.02 mmol), Cs_2CO_3 (0.4 mmol) in DMF (2.0 mL) at room temperature under irradiation with a 34 W blue LED for 12 h. The values in parenthesss represent the ratio of *syn*-addition product to *anti*-addition product determined by ^{1}H NMR and NOESY analysis. [b] The reaction was performed on a 2.0 mmol scale.

hydroxy functionalities underwent the reaction in moderate to high yields (**4a**–**4g**) with excellent stereoselectivity. Boc-protected tertiary amino acids could improve the reaction efficiency significantly, giving the corresponding products **4h** and **4i** with excellent yields and stereoselectivities. Also, Cbz-protected amino acids and common alkyl carboxylic acid were suitable substrates for this reaction.

Finally, we addressed the more challenging arylalkylation of alkynes via a photoredox/nickel dual-catalyzed three-component cross-coupling under mild reaction conditions. After evaluating various reaction parameters, the optimal reaction conditions were assigned as follows: Pc1 as photocatalyst, inexpensive $NiBr_2$ as nickel catalyst, dtbbpy as ligand, and Cs_2CO_3 as base in DMF at room temperature for 12 h. We next examined the scope with respect to the three coupling partners (Table 3). Aryl bromides bearing electron-withdrawing functional groups such as ester, ketone, and cyano underwent this three-component cross-coupling smoothly (**6a**–**6c**). Bicyclic and difunctionalized aryl bromides gave the corresponding trisubstituted alkenes in good yields (**6d** and **6e**). Strikingly, the protocol was also applied to pharmaceutically related heterocyclic and natural-product-derived aryl bromides, giving the corresponding products in good yields (**6f**–**6h**).

Regarding the scope of alkynes, electron-rich and electron-poor terminal alkynes were suitable for this transformation (**6i**–**6m**). Likewise, various Boc- and Cbz- protected cyclic and acyclic secondary amino acids, as well as a tertiary amino acid, underwent this reaction in moderate to good yields (**6m**–**6r**). Also, **6c** was obtained in 57% yield with 71:29 stereoselectivity when the reaction was performed on a 2.0 mmol scale.

To get an insight into these newly developed hydroalkylation and arylalkylation protocols, control experiments were conducted. When the reaction was conducted in deuterated acetonitrile and DMF, no deuterated product was observed (Scheme 2a). When 2 equiv D_2O was added to the reaction, the product was generated with 80:20 H/D ratio, which may be due to the formation of $CsDCO_3$ via direct or indirect H/D exchange with D_2O (Scheme 2b,c). These results show that the hydrogen atom originates from carboxylic acids via the generation of $CsHCO_3$. The isomerization efficiency for the pure *E*-isomer in the presence of Pc4 is comparable to the model hydroalkylation reaction, indicating the crucial role of the photocatalyst in the generation of the *Z*-isomer via an energy-transfer process (Scheme 2d).[12] To gain more insight into the SET process, we first performed cyclic-voltammetry (CV) measurements of Pc4 used in the

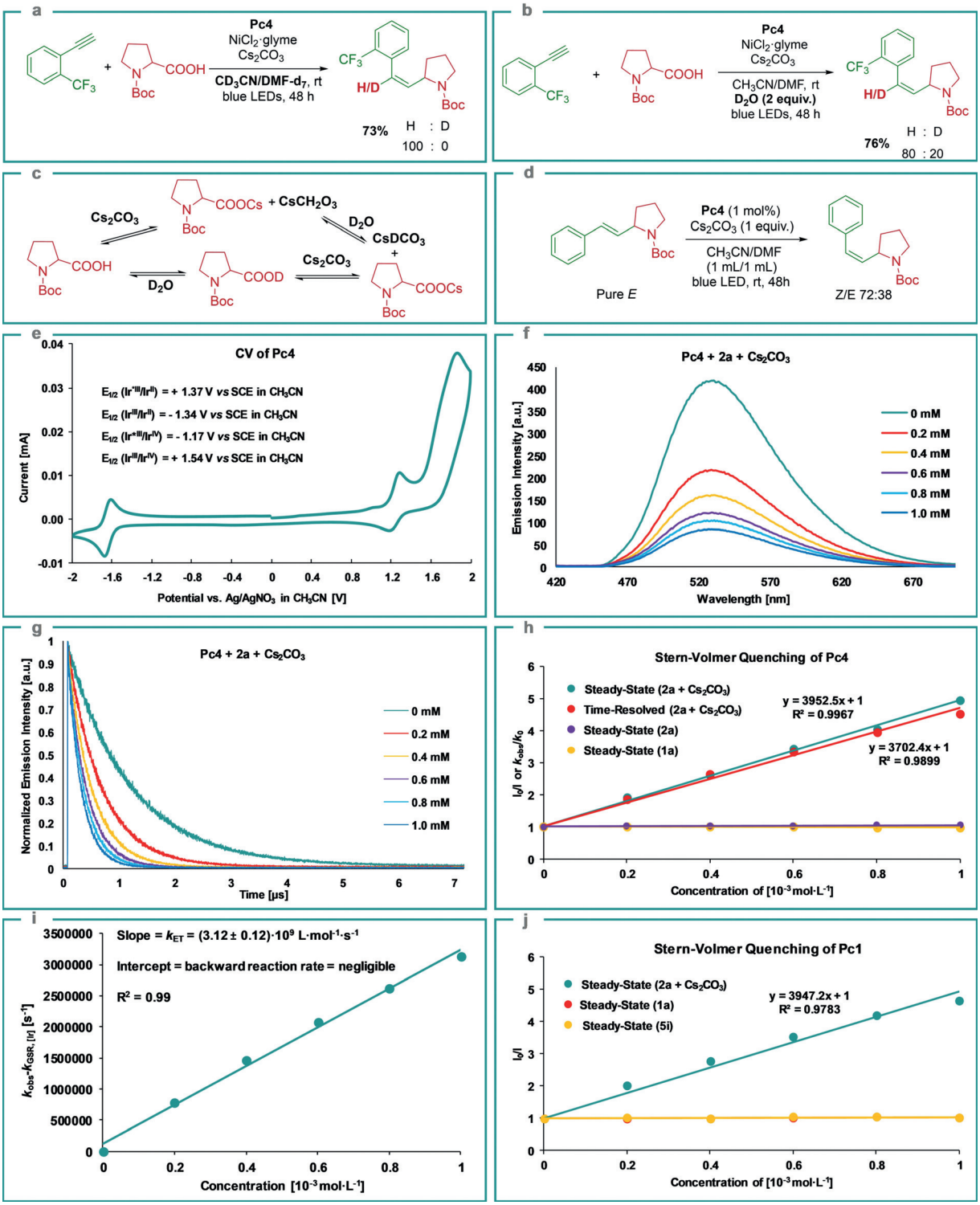

Scheme 2. Mechanistic investigation. a) Reaction conducted in CD_3CN and DMF-d^6. b) 2 equiv D_2O was added. c) Formation of $CsDCO_3$ via direct or indirect H/D exchange with D_2O. d) *Z*/*E*-isomerization via energy transfer using photocatalyst Pc4. e) CV measurement of Pc4. f) Steady-state Stern–Volmer experiment of Pc4 and Boc-Pro-OCs (**2a** + Cs_2CO_3). g) Phosphorescence lifetimes of ^{3*}Pc4 at different concentrations of quencher (**2a** + Cs_2CO_3). h) Combined quenching data of steady-state and time-resolved studies of Pc4. i) Stern–Volmer analysis yielded a rate constant, k_{ET}, of $(3.12 \pm 0.12) \times 10^9$ L mol^{-1} s^{-1} by the SET between ^{3*}Pc4 and Boc-Pro-OCs (**2a** + Cs_2CO_3). The backward reaction rate is negligible. j) Steady-state Stern–Volmer quenching analysis of Pc1 in the presence of Boc-Pro-OCs (**2a** + Cs_2CO_3), phenylacetylene **1a** or *p*-bromoacetophenone **5i**.

hydroalkylation reactions (Scheme 2e). The reduction potential of the triplet excited-state photocatalyst ^{3*}Pc4 [$E_{1/2}$(Ir*^{III}/Ir^{II}) = +1.37 V vs. SCE in CH_3CN][13] is thermodynamically favored to induce the single-electron oxidation of deprotonated α-amino acids (Boc-Pro-OCs ($E_{1/2}$ = +0.95 V vs. SCE in CH_3CN).[9e] Next, steady-state Stern–Volmer luminescence-

quenching experiments were conducted by the addition of various concentrations of substrates (**2a** or **1a**) to Pc4. The results show that the photocatalyst Pc4 was not quenched (Scheme 2h). However, the deprotonated **2a** (**2a** + Cs_2CO_3) quenched the photocatalyst Pc4 (Scheme 2f) and the Stern–Volmer plot displayed a linear correlation (Scheme 2h), showing the importance of the base in the generation of the alkyl radical. Additionally, a lifetime measurement of ^{3*}Pc4 using time-resolved emission spectroscopy was also carried out. Here, a relatively stable and long-lived ^{3*}Pc4 was observed (1127 ns, Figure S11 in the Supporting Information) which decreased monotonously with the increase in quencher concentration (**2a** + Cs_2CO_3; Scheme 2g). Furthermore, the slopes of the steady-state and time-resolved Stern–Volmer plots are very similar (Scheme 2h), indicating that the major quenching process is the dynamic quenching of excited-state ^{3*}Pc4 by Boc-Pro-OCs.[14] Also, the electron-transfer (ET) rate constant k_{ET} was determined by plotting difference between the observed rate constant (k_{obs}) and the ground-state recovery rate (k_{GSR}) vs. different concentrations of quencher (**2a** + Cs_2CO_3). A slope of $(3.12 \pm 0.12) \times 10^9\ L\,mol^{-1}\,s^{-1}$ was observed, which correlates with the ET

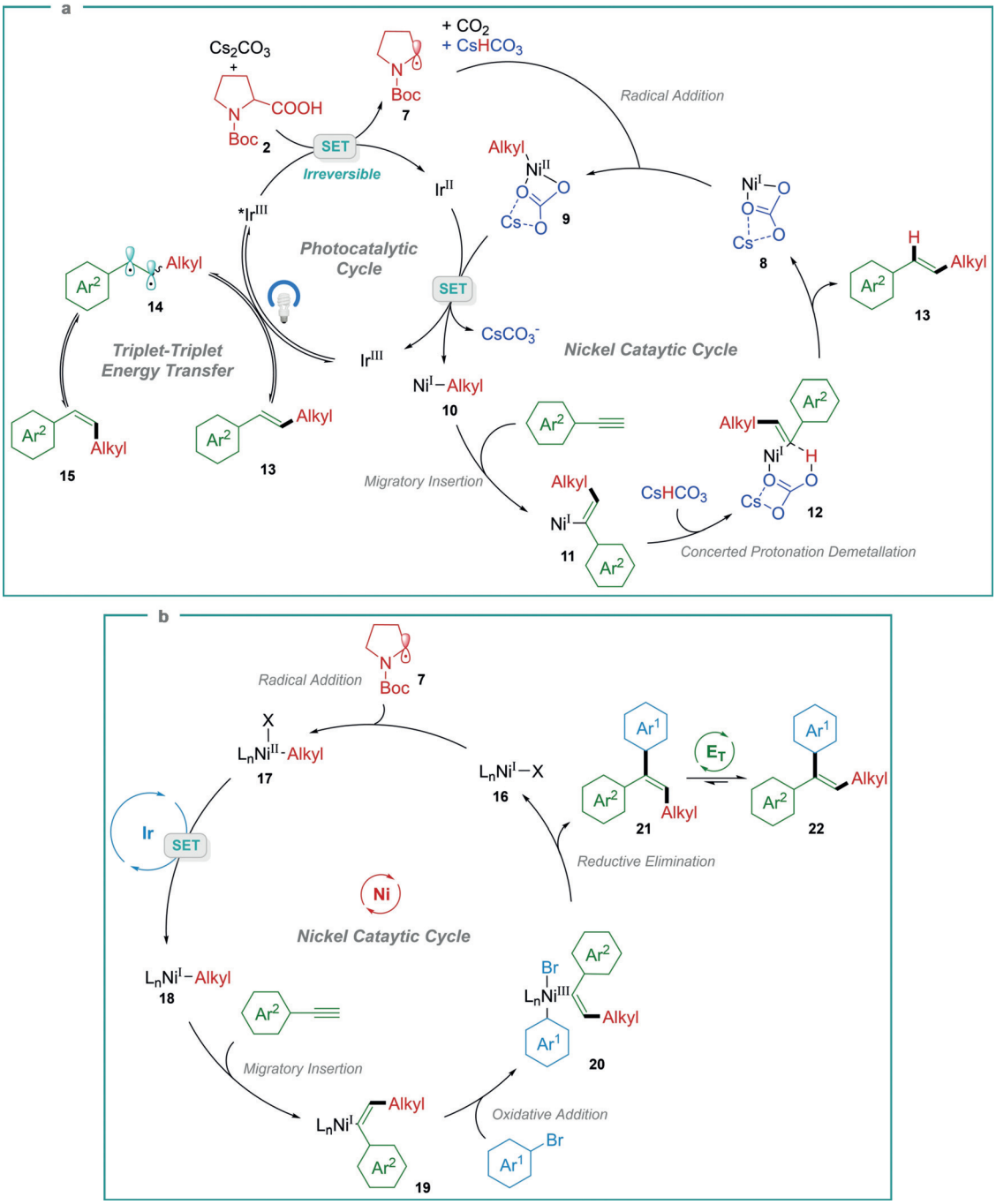

Scheme 3. Proposed mechanism for the photoredox/nickel dual-catalyzed a) hydroalkylation and b) arylalkylation of alkynes.

rate constant, k_{ET}, for **2a** and Pc4, while the intercept represents the backward reaction rate (Scheme 2i), which is negligible, showing that this SET process is irreversible.[15]

Furthermore, a steady-state quenching experiment showed that the photocatalyst Pc1 used in arylalkylation reactions was quenched by Boc-Pro-OCs, while it was not quenched by phenylacetylene **1a** and *p*-bromoacetophenone **5i** (Scheme 2j). Based on these results, mechanisms for the photoredox/nickel dual-catalyzed hydroalkylation and arylalkylation of alkynes are proposed (Scheme 3a,b). First, the Ir^{III} complex absorbs visible light and forms a long-lived triplet excited state $*Ir^{III}$ complex.[8b] Oxidation of the carboxylic acid by the $*Ir^{III}$ complex and subsequent CO_2 extrusion generates the alkyl radical intermediate **7**,[9e] which is trapped by the Ni^{I} complex **8** to afford Ni^{II} intermediate **9**. Reduction of **9** by the Ir^{II} reductant gives Ni^{I} intermediate **10**, which undergoes 1,2-migratory alkyne insertion to form Ni^{I} intermediate **11**.[11,16] For the hydroalkylation process, protonation of **11** via intermediate **12** generates the *E*-isomer **13** (concerted protonation demetallation, CPD) along with the formation of Ni^{I} complex **8**.[17] Next, the *Z*-isomer **15** is obtained via intermediate **14** from the *E*-isomer **13** through an energy-transfer pathway (Scheme 3a).[3c] Likewise, for arylalkylation, the generated Ni^{I} intermediate **19** undergoes the oxidative addition of an aryl halide to give intermediate **20**, followed by reductive elimination to deliver the *anti*-addition three-component coupling product **21**. At last, the *syn*-addition three-component coupling product **22** is obtained via the energy-transfer pathway (Scheme 3b).[3c]

Furthermore, DFT calculations for the migratory-insertion and the concerted protonation–demetallation steps were conducted to rationalize and support the proposed mechanism (Scheme 4a). As a model reaction, we investigated the cross-coupling between phenylacetylene **1a** and Boc-Pro-OH **2a**. The migratory insertion step commenced with the coordination of phenylacetylene to the active alkyl-Ni^{I} catalyst A, forming the intermediate complex B. Next, the alkyl group at the nickel center migrates to the terminal carbon atom of the alkyne to generate the Ni^{I} intermediate C via the transition state B-TS with an energy barrier of only 6.3 kcal mol^{-1}. In the next step, $CsHCO_3$ coordinates to the formed Ni^{I} intermediate C to give Ni^{I} complex D, followed by the concerted protonation–demetallation to form the Ni^{I} intermediate E via the transition state D-TS. Finally, the

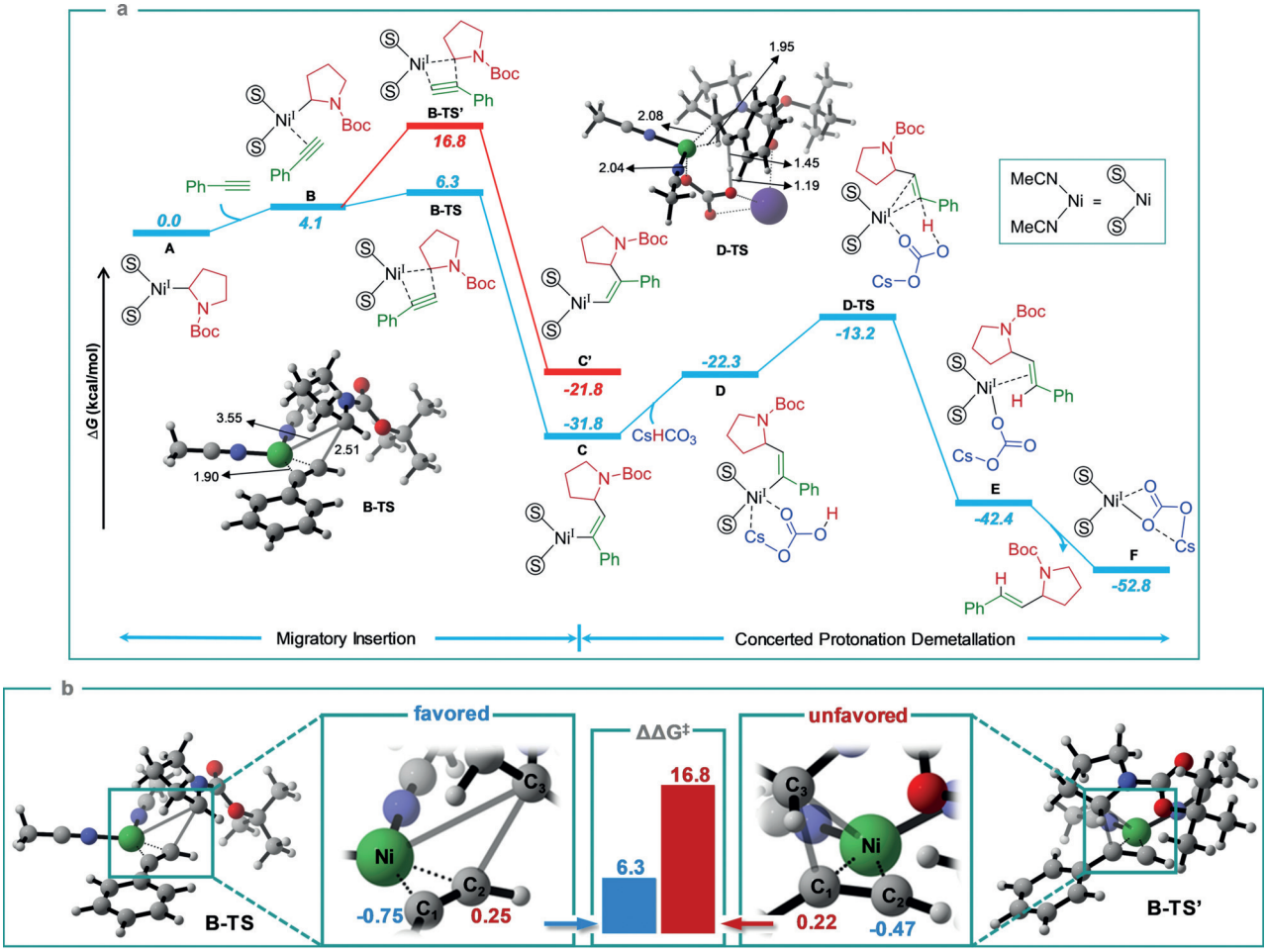

Scheme 4. a) DFT-computed energy profiles for the migratory insertion and concerted protonation–demetallation steps. Free energies in solution (in kcal mol^{-1}) calculated at SMD(acetonitrile)-M06/Def2-TZVPP//PBE/Def2-TZVP(Ni)/Def2-SVP (other atoms) Selected optimized geometries are shown. Bond lengths in Å. b) Energy barrier for migratory insertion with different regioselectivities and the ADCH atomic charges of carbon atoms C1 and C2 at the transition states.

product is liberated along with the formation of the Ni^{I} complex F with a free energy gain of 10.4 kcal mol^{-1}. Alternatively, the pathway in which the alkyl group at the nickel center migrates to the internal carbon atom of the alkyne was also calculated. The energy barrier of this pathway is 16.8 kcal mol^{-1} (B-TS′), which is highly unfavorable compared the 6.3 kcal mol^{-1} of B-TS. Additionally, the migratory insertion of the alkyne at the Ni^{II} center was calculated, which also shows *anti*-Markovnikov regioselectivity; however, the energy barrier is considerably higher (Figure S13). To further explain the regioselectivity of the migratory insertion step, wavefunction analysis was conducted to calculate the ADCH (atomic-dipole-moment-corrected Hirshfeld) atomic charge[18] of the C(sp)-carbon atoms C1 and C2 in the transition states B-TS and B-TS′ (Scheme 4 b).[19] The results show that in the transition state B-TS, the atomic charges for C1 and C2 are −0.75 and + 0.25 a.u., respectively, while in the transition state B-TS′, C2 and C1 have atomic charges of −0.47 and + 0.22 a.u., respectively. Thus, the alkyl group is prone to migrate to C2 in B-TS as it is more electrophilic than C1 in B-TS′, and at the same time, C1 in B-TS is considerably more nucleophilic than C2 in B-TS′ and thus easier to bind to the nickel center.

Conclusion

In conclusion, the hydroalkylation and arylalkylation of alkynes presented herein is an efficient approach for the synthesis of a series of highly valuable disubstituted and trisubstituted alkenes via photoredox/nickel dual catalysis which takes place under mild reaction conditions. Both protocols possess a broad substrate scope including complex starting materials and good functional-group tolerance. Notably, the reactions take place efficiently, with excellent regioselectivity and moderate-to-excellent stereoselectivity (*syn*-addition manner). Steady-state and time-resolved fluorescence-spectroscopy measurements were conducted, confirming the dynamic quenching between the photocatalyst and deprotonated amino acid. Additionally, DFT calculations as well as wavefunction analysis were performed to reveal the regioselectivity of the migratory insertion step. Owing to the broad substrate scope and successful scale-up, these protocols should find application in the synthesis of highly valuable disubstituted and trisubstituted alkenes.

Acknowledgements

C.Z. acknowledges the King Abdullah University of Science and Technology (KAUST) for support and the KAUST Supercomputing Laboratory for providing computational resources of the supercomputer Shaheen II. The research leading to these results has received funding from the European Research Council under the European Union's Seventh Framework Programme (FP/2007–2013)/ERC Grant Agreement no. 617044 (SunCatChem).

Conflict of interest

The authors declare no conflict of interest.

Keywords: alkynes · arylalkylation · DFT calculations · hydroalkylation · nickel · photoredox reactions

How to cite: *Angew. Chem. Int. Ed.* **2020**, *59*, 5738–5746
Angew. Chem. **2020**, *132*, 5787–5795

[1] a) L. F. Tietze, A. Modi, *Med. Res. Rev.* **2000**, *20*, 304–322; b) G. Masson, L. Neuville, C. Bughin, A. Fayol, J. Zhu, *Top. Heterocycl. Chem.* **2010**, 1–24; c) A. Dömling, W. Wang, K. Wang, *Chem. Rev.* **2012**, *112*, 3083–3135; d) J. Zhu, Q. Wang, M. Wang, *Multicomponent reactions in organic synthesis*, Wiley-VCH, Weinheim, **2015**; e) L. Levi, T. J. Mueller, *Chem. Soc. Rev.* **2016**, *45*, 2825–2846.

[2] T. J. J. Müller, K. Deilhof, in *Multicomponent Reactions in Organic Synthesis* (Eds.: J. Zhu, Q. Wang, M.-X. Wang), Wiley-VCH, Weinheim, **2015**, pp. 333–378.

[3] a) Z. Li, A. García-Domínguez, C. Nevado, *J. Am. Chem. Soc.* **2015**, *137*, 11610–11613; b) Z. Li, A. García-Domínguez, C. Nevado, *Angew. Chem. Int. Ed.* **2016**, *55*, 6938–6941; *Angew. Chem.* **2016**, *128*, 7052–7055; c) L. Guo, F. Song, S. Zhu, H. Li, L. Chu, *Nat. Commun.* **2018**, *9*, 4543; d) C. Zhu, H. Yue, B. Maity, I. Atodiresei, L. Cavallo, M. Rueping, *Nat. Catal.* **2019**, *2*, 678–687.

[4] a) P. Wipf, D. L. Waller, J. T. Reeves, *J. Org. Chem.* **2005**, *70*, 8096–8102; b) C. W. Cheung, X. Hu, *Chem. Eur. J.* **2015**, *21*, 18439–18444.

[5] a) R. Chinchilla, C. Najera, *Chem. Rev.* **2014**, *114*, 1783–1826; b) B. M. Trost, C.-J. Li, *Modern alkyne chemistry: Catalytic and atom-economic transformations*, Wiley-VCH, Weinheim, **2014**.

[6] a) T. Kitamura, *Eur. J. Org. Chem.* **2009**, 1111–1125; b) Y. Yamamoto, *Chem. Soc. Rev.* **2014**, *43*, 1575–1600; c) V. P. Boyarskiy, D. S. Ryabukhin, N. A. Bokach, A. V. Vasilyev, *Chem. Rev.* **2016**, *116*, 5894–5986.

[7] a) C. W. Cheung, F. E. Zhurkin, X. Hu, *J. Am. Chem. Soc.* **2015**, *137*, 4932–4935; b) J. Li, J. Zhang, H. Tan, D. Z. Wang, *Org. Lett.* **2015**, *17*, 2522–2525; c) A. M. Suess, M. R. Uehling, W. Kaminsky, G. Lalic, *J. Am. Chem. Soc.* **2015**, *137*, 7747–7753; d) M. R. Uehling, A. M. Suess, G. Lalic, *J. Am. Chem. Soc.* **2015**, *137*, 1424–1427; e) Y. Li, L. Ge, B. Qian, K. R. Babu, H. Bao, *Tetrahedron Lett.* **2016**, *57*, 5677–5680; f) X.-Y. Lu, J.-H. Liu, X. Lu, Z.-Q. Zhang, T.-J. Gong, B. Xiao, Y. Fu, *Chem. Commun.* **2016**, *52*, 5324–5327; g) X. H. Ouyang, R. J. Song, B. Liu, J. H. Li, *Adv. Synth. Catal.* **2016**, *358*, 1903–1909; h) K. Nakamura, T. Nishikata, *ACS Catal.* **2017**, *7*, 1049–1052.

[8] a) M. Parasram, V. Gevorgyan, *Chem. Soc. Rev.* **2017**, *46*, 6227–6240; b) J. Twilton, P. Zhang, M. H. Shaw, R. W. Evans, D. W. MacMillan, *Nat. Rev. Chem.* **2017**, *1*, 0052; c) H. Huo, X. Shen, C. Wang, L. Zhang, P. Röse, L.-A. Chen, K. Harms, M. Marsch, G. Hilt, E. Meggers, *Nature* **2014**, *515*, 100–103; d) Q. Meng, T. Schirmer, K. Katou, B. König, *Angew. Chem. Int. Ed.* **2019**, *58*, 5723–5728; *Angew. Chem.* **2019**, *131*, 5779–5784; e) L. Zhang, X. Si, Y. Yang, M. Zimmer, S. Witzel, K. Sekine, M. Rudolph, A. S. K. Hashmi, *Angew. Chem. Int. Ed.* **2019**, *58*, 1823–1827; *Angew. Chem.* **2019**, *131*, 1837–1841.

[9] Examples: a) L. N. Cavalcanti, G. A. Molander, *Top. Curr. Chem.* **2016**, *362*, 1–23; b) J. C. Tellis, C. B. Kelly, D. N. Primer, M. Jouffroy, N. R. Patel, G. A. Molander, *Acc. Chem. Res.* **2016**, *49*, 1429–1439; c) J. A. Milligan, J. P. Phelan, S. O. Badir, G. A. Molander, *Angew. Chem. Int. Ed.* **2019**, *58*, 6152–6163; *Angew. Chem.* **2019**, *131*, 6212–6224; d) J. C. Tellis, D. N. Primer, G. A.

Molander, *Science* **2014**, *345*, 433 – 436; e) Z. Zuo, D. T. Ahneman, L. Chu, J. A. Terrett, A. G. Doyle, D. W. MacMillan, *Science* **2014**, *345*, 437 – 440; f) S. Zheng, Á. Gutiérrez-Bonet, G. A. Molander, *Chem* **2019**, *5*, 339 – 352; g) J. K. Matsui, Á. Gutiérrez-Bonet, M. Rotella, R. Alam, O. Gutierrez, G. A. Molander, *Angew. Chem. Int. Ed.* **2018**, *57*, 15847 – 15851; *Angew. Chem.* **2018**, *130*, 16073 – 16077; h) A. Dumoulin, J. K. Matsui, Á. Gutiérrez-Bonet, G. A. Molander, *Angew. Chem. Int. Ed.* **2018**, *57*, 6614 – 6618; *Angew. Chem.* **2018**, *130*, 6724 – 6728; i) J. Li, Y. Luo, H. W. Cheo, Y. Lan, J. Wu, *Chem* **2019**, *5*, 192 – 203; j) V. Corcé, L. M. Chamoreau, E. Derat, J. P. Goddard, C. Ollivier, L. Fensterbank, *Angew. Chem. Int. Ed.* **2015**, *54*, 11414 – 11418; *Angew. Chem.* **2015**, *127*, 11576 – 11580; k) M. S. Oderinde, N. H. Jones, A. Juneau, M. Frenette, B. Aquila, S. Tentarelli, D. W. Robbins, J. W. Johannes, *Angew. Chem. Int. Ed.* **2016**, *55*, 13219 – 13223; *Angew. Chem.* **2016**, *128*, 13413 – 13417; l) M. S. Oderinde, M. Frenette, D. W. Robbins, B. Aquila, J. W. Johannes, *J. Am. Chem. Soc.* **2016**, *138*, 1760 – 1763; m) L. Fan, J. Jia, H. Hou, Q. Lefebvre, M. Rueping, *Chem. Eur. J.* **2016**, *22*, 16437 – 16440; n) H. Yue, C. Zhu, M. Rueping, *Angew. Chem. Int. Ed.* **2018**, *57*, 1371 – 1375; *Angew. Chem.* **2018**, *130*, 1385 – 1389; o) L. Huang, M. Rueping, *Angew. Chem. Int. Ed.* **2018**, *57*, 10333 – 10337; *Angew. Chem.* **2018**, *130*, 10490 – 10494; p) R. Kancherla, K. Muralirajan, S. Arunachalam, M. Rueping, *Trends Chem.* **2019**, *1*, 510 – 523; q) A. Dewanji, P. E. Krach, M. Rueping, *Angew. Chem. Int. Ed.* **2019**, *58*, 3566 – 3570; *Angew. Chem.* **2019**, *131*, 3604 – 3608; r) L. Huang, C. Zhu, L. Yi, H. Yue, R. Kancherla, M. Rueping, *Angew. Chem. Int. Ed.* **2020**, *59*, 457 – 464; *Angew. Chem.* **2020**, *132*, 465 – 472.

[10] H.-P. Deng, X.-Z. Fan, Z.-H. Chen, Q.-H. Xu, J. Wu, *J. Am. Chem. Soc.* **2017**, *139*, 13579 – 13584.

[11] N. A. Till, R. T. Smith, D. W. MacMillan, *J. Am. Chem. Soc.* **2018**, *140*, 5701 – 5705.

[12] K. Singh, S. J. Staig, J. D. Weaver, *J. Am. Chem. Soc.* **2014**, *136*, 5275 – 5278.

[13] The reduction potential of triplet excited state photocatalyst ^{3*}Pc4 was obtained by converting the ground-state redox potential to the excited-state redox pontential; see the Supporting Information for more details.

[14] D. M. Arias-Rotondo, J. K. McCusker, *Chem. Soc. Rev.* **2016**, *45*, 5803 – 5820.

[15] a) P. Nuhant, M. S. Oderinde, J. Genovino, A. Juneau, Y. Gagné, C. Allais, G. M. Chinigo, C. Choi, N. W. Sach, L. Bernier, Y. M. Fobian, M. W. Bundesmann, B. Khunte, M. Frenette, O. O. Fadeyi, *Angew. Chem. Int. Ed.* **2017**, *56*, 15309 – 15313; *Angew. Chem.* **2017**, *129*, 15511 – 15515; b) M. Teders, C. Henkel, L. Anhäuser, F. Strieth-Kalthoff, A. Gómez-Suárez, R. Kleinmans, A. Kahnt, A. Rentmeister, D. Guidi, F. Glorius, *Nat. Chem.* **2018**, *10*, 981 – 988.

[16] J. M. Huggins, R. G. Bergman, *J. Am. Chem. Soc.* **1981**, *103*, 3002 – 3011.

[17] B. Maity, D. Koley, *ChemCatChem* **2018**, *10*, 566 – 580.

[18] a) T. Lu, F. Chen, *J. Theor. Comput. Chem.* **2012**, *11*, 163 – 183; b) T. Lu, F. Chen, *Acta Phys. Chim. Sin.* **2012**, *28*, 1 – 18.

[19] ADCH atomic charges were calculated by Multiwfn 3.7. see: T. Lu, F. Chen, *J. Comput. Chem.* **2012**, *33*, 580 – 592.

Manuscript received: November 5, 2019
Revised manuscript received: December 20, 2019
Accepted manuscript online: January 4, 2020
Version of record online: February 3, 2020

